SCIENTIFIC REPORTS

Anomalous orbital structure in two-dimensional titanium dichalcogenides

Banabir Pal[1], Yanwei Cao[1,2], Xiaoran Liu[1], Fangdi Wen[1], M. Kareev[1], A. T. N'Diaye[3], P. Shafer[3], E. Arenholz[3] & J. Chakhalian[1]

Generally, lattice distortions play a key role in determining the electronic ground states of materials. Although it is well known that trigonal distortions are generic to most two dimensional transition metal dichalcogenides, the impact of this structural distortion on the electronic structure and topological properties has not been understood conclusively. Here, by using a combination of polarization dependent X-ray absorption spectroscopy (XAS), X-ray photoelectron spectroscopy (XPS) and atomic multiplet cluster calculations, we have investigated the electronic structure of titanium dichalcogenides TiX_2 (X = S, Se, Te), where the magnitude of the trigonal distortion increase monotonically from S to Se and Te. Our results reveal the presence of an anomalously large crystal field splitting. This unusual kind of crystal field splitting is likely responsible for the unconventional electronic structure of TiX_2 compounds and ultimately controls the degree of the electronic phase protection. Our findings also indicate the drawback of the distorted crystal field picture in explaining the observed electronic ground state and emphasize the key importance of trigonal symmetry, metal-ligand hybridization and electron-electron correlations in defining the electronic structures at the Fermi energy.

The realization of numerous exotic electronic phases of graphene[1–3] and the relentless tendency to miniaturization of silicon-based electronics[4] have ignited exhaustive research in a wide range of two dimensional (2D) layered materials. As a result, 2D transition metal dichalcogenides have emerged as the promising platform with intriguing topological and electronic ground states and high potential for applicability in the field of microelectronics[5,6], nanophotonics[7,8], optoelectronics[9,10] and photovoltaics[11–13] to name a few.

A generic feature of this dichalcogenide family is the presence of structural distortions which play a critical role in defining the electronic ground state and invariably the topological properties of these systems. Specifically, the lattice deformations can strongly alter the interatomic interaction strength and thereby are responsible for various novel electronic phases including charge density wave in VSe_2[14,15], $NbSe_2$[16] and $TaSe_2$[17,18], superconductivity in $FeSe_{1-x}Te_x$[19], insulating ground states in $ReSe_2$[20], Weyl semi-metallic phase in $MoTe_2$[21] and many more. On the other hand, recent results on topological phases (TPs) have demonstrated a remarkable degree of protection against perturbations as long as the key symmetries remain intact[22]. Experimentally, surprisingly very little is know about the TP stability subjected to lattice distortions associated with trigonal symmetry as trigonal distortions could be used to either enter a topological phase, or exit a topological phase with a trigonal distortion[22–25]. Naturally, a way to microscopically probe and understand the effect of lattice deformations, induced covalency, and electron-electron correlations along with their impact on the electronic structure are essential for deterministic control of the rich physical phases of these TMDs compounds.

Recently, titanium dichalcogenides TiX_2 (here X = S, Se and Te) have attracted significant attention of the community as the exemplary TMD systems[26–30]. While the usual crystallographic form of TiX_2 is the layered CdI_2 type[31], these systems also possess a distinct trigonal distortion from an ideal octahedral crystal environment[31,32]. Previously, detailed structural investigation established that the magnitude of the distortion varies monotonically from nearly octahedral in TiS_2[31] to highly distorted in $TiTe_2$[32]. In addition, large body of work on transition metal compounds suggest that these generic trigonal distortions may have strong influence in modifying the energy

[1]Department of Physics and Astronomy, Rutgers University, Piscataway, New Jersey, 08854, USA. [2]Ningbo Institute of Materials Technology and Engineering, Chinese Academy of Sciences, Ningbo, Zhejiang, 315201, China. [3]Advanced Light Source, Lawrence Berkley National Laboratory, Berkeley, California, 94720, USA. Correspondence and requests for materials should be addressed to B.P. (email: bp435@physics.rutgers.edu) or Y.C. (email: ywcao@nimte.ac.cn)

1
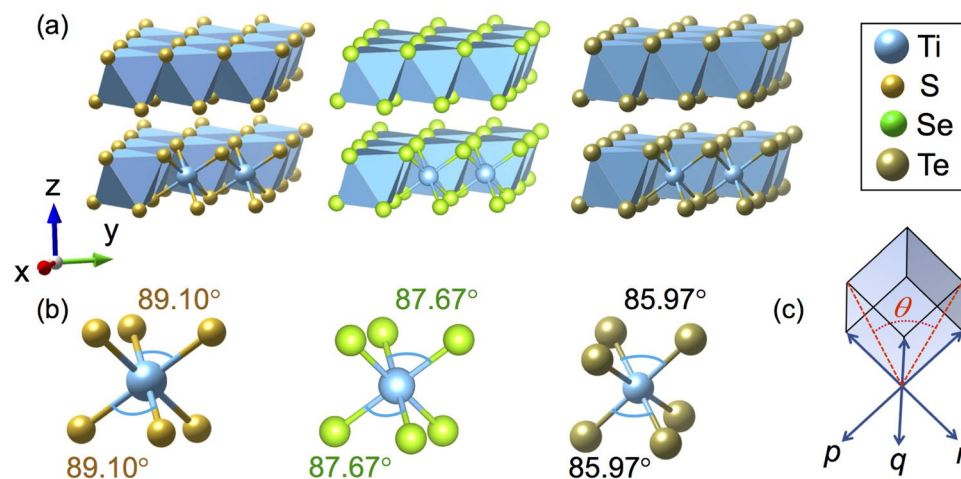
Figure 1. (**a**) Schematic crystal structure of the TiS_2, $TiSe_2$, and $TiTe_2$ compounds showing nearly octahedral environment of each TiX_2 unit. (**b**) Distortion of the ideal octahedral environment across the chalcogenide series. It is to be noted that the distortion does not change the bond length but alters the bond angle. (**c**) Schematic representation of the trigonal distortions.

level and electronic structure of the chalcogenides. The problem is vividly illustrated by the case of $TiSe_2$ which undergoes the transition into a chiral charge density wave (CDW) state[33,34] and further into a conventional CDW resulting in dramatic renormalization of electronic and structural properties. The fundamental challenge here is to separate the many-body effects associated with excitonic condensate[35–37] from the Jahn-Teller like instability from the strong-electron phonon coupling[38,39]. In addition, recent extensive theoretical work based on LDA + U[40] along with the detailed ARPES[41] study hinted on the importance of lattice distortions coupled with strong electron-electron correlations to explain the ground state properties of $TiSe_2$. Based on those findings and given the obvious importance of these the whole TiX_2 family, there have been several experimental and theoretical investigations to understand the impact of trigonal distortion on the electronic structure in these systems[42–44]. However, in absence of systematic spectroscopic investigations corroborated with theoretical calculations the consequence of the trigonal distortion on the electronic structure of the TiX_2 systems has not convincingly been reported thus far. Here, we have addressed this issue by investigating the whole family of TiX_2 single crystals by means of polarization dependent X-ray absorption spectroscopy in conjunction with the multiplet cluster calculations. Our results unambiguously demonstrate the failure of the standard ionic configuration and distorted crystal field picture in predicting electronic ground states and thereby reveal the key importance of metal-ligand hybridization between titanium and chalcogen ions and electronic correlations in defining their electronic properties.

Results and Discussion

As shown in Fig. 1(a), all members of the TiX_2 family crystallize into trigonal CdI_2 type layered structure with space group P_{3m1}[31]. The crystal structure consists of repeated tri-layers (Fig. 1(a)) along crystallographic z direction; each tri-layer in these systems contains a titanium layer sandwiched between two layers of chalcogenides. Although the interactions between titanium and chalcogenides are strong within a tri-layer, the chalcogen bonding between two tri-layers is weak and dominated by the weak van der Waals type interaction. Each tri-layer further experiences an elongated trigonal distortion where all six Ti-X bond length remains constant but X-Ti-X bond angle deviates from an ideal 90° in such a manner that the crystallographic lattice parameter along z direction increases in length. As illustrated in Fig. 1(b) the strength of elongated trigonal distortion increases monotonically from TiS_2 to $TiTe_2$ with three different X-Ti-X bond angles. The magnitude of such elongated trigonal distortion can be estimated from c/a ratio where c and a represent the corresponding unit cell parameter along z and x direction, respectively; For an ideal octahedral environment, the c/a ratio is close to 1.633 whereas the c/a ratio for TiS_2, $TiSe_2$ and $TiTe_2$ are found to be 1.726, 1.732 and 1.808, respectively. This type of structural distortion can also be alternatively explained in terms of the distortion angle Θ between the diagonals of the pq, qr, rp plane as schematically shown in Fig. 1(c). For a regular octahedron $\Theta = 60°$ and becomes lesser and greater than 60° for elongated and compressive trigonal distortions, respectively.

Chemical quality, and the absence of chalcogen vacancies critical for most dichalcogenides are verified by X-ray photo electron spectroscopy (XPS) measurements carried out on freshly cleaved TiX_2 single crystals to rule out the presence of any anion vacancies. The basic process associated with the XPS technique is shown schematically in Fig. 2(a). Generally, the chemical shift associated with each core level provides important information about the charge state of the different elements of the system under investigation. Figure 2(b) displays typical Ti $2p$ core level spectra for three different TiX_2 systems (Core level XPS spectra of Chalcogenides are shown in Supporting Information). Each Ti $2p$ core-level spectrum shown in Fig. 2(b) is composed of two intense spin-orbit split doublet (marked as A and B) with a spin-orbit splitting strength close to 5.8 eV. Feature A appearing at a binding energy range between 454 eV to 459 eV represents Ti $2p_{3/2}$ like states whereas feature B arises mainly from Ti $2p_{1/2}$ like states. Interestingly, a systematic shift in peak position was found from higher to lower binding energy in Ti $2p$ core level spectra from TiS_2 to $TiTe_2$, respectively. These shifts in the binding energy were
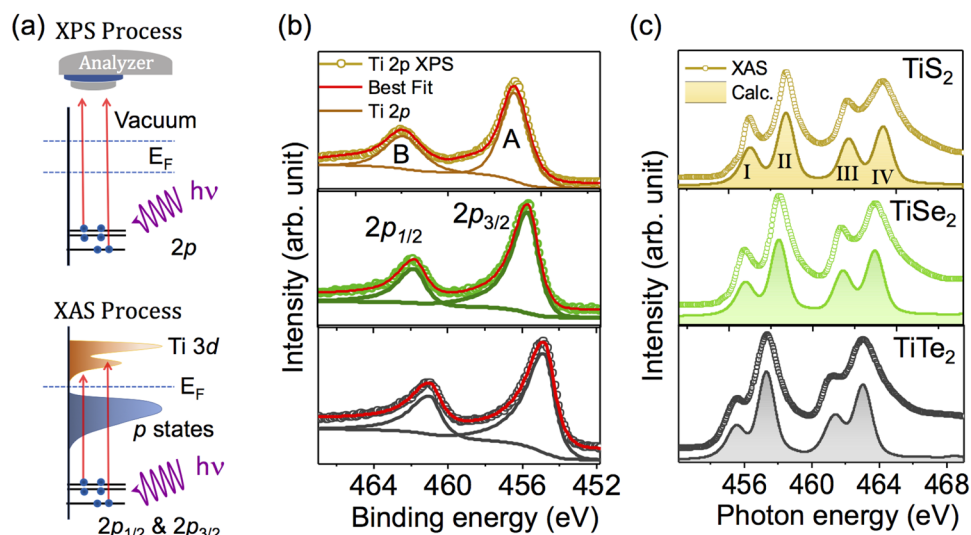
Figure 2. (**a**) Schematic representations of the X-ray photoelectron (top) and X-ray absorption (bottom) spectroscopy process. (**b**) X-ray photoelectron spectra of Ti 2p core level. Each spectrum was decomposed with Lorentzian function convoluted with Gaussian functions. (**c**) Experimental XAS spectra (open circle) of three different TiX$_2$ systems were compared with atomic multiplet calculations (shaded area).

previously attributed to the reduction in ionic contribution in Ti-X chemical bond formations[45]. In this work, each spectrum was decomposed using a Gaussian-Lorentz line profile and a Shirley type background function and can be accounted within a single Gaussian-Lorentz line profile. The absence of the multiple peak structure in Ti 2p core level spectra clearly implies the presence single valence Ti, and rules out any signature of anion vacancies in our TiX$_2$ samples.

To investigate the evolutions in electronic structure across the TiX$_2$ series, XAS measurements were carried out on Ti L$_{2,3}$ edge at beamline 4.0.2 of the Advanced Light Source, at Lawrence Berkeley National Laboratory. In a typical Ti L$_{3,2}$ XAS process (see bottom of Fig. 2(a)), electrons are excited from Ti 2p core level (from 2$p_{3/2}$ and 2$p_{1/2}$) to the Ti 3d conduction band; each L$_{3,2}$ XAS spectrum splits into two edges (L$_2$ and L$_3$) due to the spin-orbit coupling of Ti 2p states. Experimentally obtained Ti L$_{2,3}$ XAS spectra for three different TiX$_2$ systems are shown in Fig. 2(c) as open circles. As seen both L$_3$ and L$_2$ peaks of each spectrum exhibit a double hump feature arising primarily from nearly octahedral crystal field effects which splits the fivefold degenerate 3d orbitals of Ti into doubly degenerate e_g and triply degenerate t_{2g} orbitals. For a quantitative understanding, theoretical atomic multiplet cluster calculations were performed within a TiX$_6$ cluster with O$_h$ point group symmetry and Ti^{4+} ionic configuration[46]. The obtained calculated spectra are shown as shaded line in Fig. 2(c) confirm that only one types of charge state Ti^{4+} is present in our samples. In good agreement with the XPS spectra, we observed a gradual shift in the XAS spectra from TiS$_2$ to TiTe$_2$. This monotonic spectral shift suggests a systematic decrease in $(U_{dd} - U_{pd})$ from TiS$_2$ to TiTe$_2$ where U_{dd} symbolizes the onsite coulomb interaction strength and U_{pd} defines the core hole interaction potential. This result indicates that in case of Te, the strongest interatomic $p - d$ interaction strength arises from the markedly increased metal-ligand hybridization. The summary of the relative energy position of the occupied 2p states and unoccupied 3d states of titanium obtained from XPS and XAS measurements is given schematically in Fig. 3.

Despite high XAS sensitivity to charge state and local symmetry, it is still very challenging to capture the effect of trigonal distortions from non-polarized XAS measurement. To further explore the impact of trigonal distortion, detailed polarization dependent XAS measurements were carried out. Polarization dependent XAS process can probe local orbital character depending on their relative orientation with respect to crystallographic axes; for example it can be sensitive to the sub-band splitting of t_{2g} states which may emerge from local lattice distortions. The process associated with the polarization dependent XAS (in-plane vs. out-of-plane) are schematically shown in Fig. 4(a). Since our samples are aligned along their natural [111] direction (z axis in Fig. 1(a) is along [111] direction), it is expected that out-of-plane polarization will be sensitive to the orbitals oriented along [111] direction whereas the in-plane polarization will probe those states which are oriented perpendicular to the [111] directions. Both out-of-plane (H) and in-plane (V) polarization dependent spectra are shown in Fig. 4(b). As immediately seen, a clear difference between the in- and out-of-plane XAS spectra is present which in turn implies the presence of distinct d-orbital anisotropy. The corresponding XLD signal or the difference between the in- and out-of-plane XAS spectrum is shown as the shaded area in Fig. 4(b) for all three samples.

To make a connection between the XLD results and orbital occupation we discuss electronic structure of the TiX$_2$ compounds. In the purely ionic limit, the electronic structure of these systems comprises of fully occupied p states of chalcogen atom (S or Se or Te) forming valence bands and unoccupied conduction bands with the predominant Ti 3d character. Due to the effect of octahedral crystal field, five-fold degenerate 3d orbitals of Ti split into a doubly degenerate higher energy e_g and a triply degenerate lower energy t_{2g} states[32]. In addition, as shown schematically in Fig. 4(c) due to elongated trigonal distortion[47] t_{2g} states further split into a higher energy singlet a_{1g} and lower energy doublet e_g^π states.
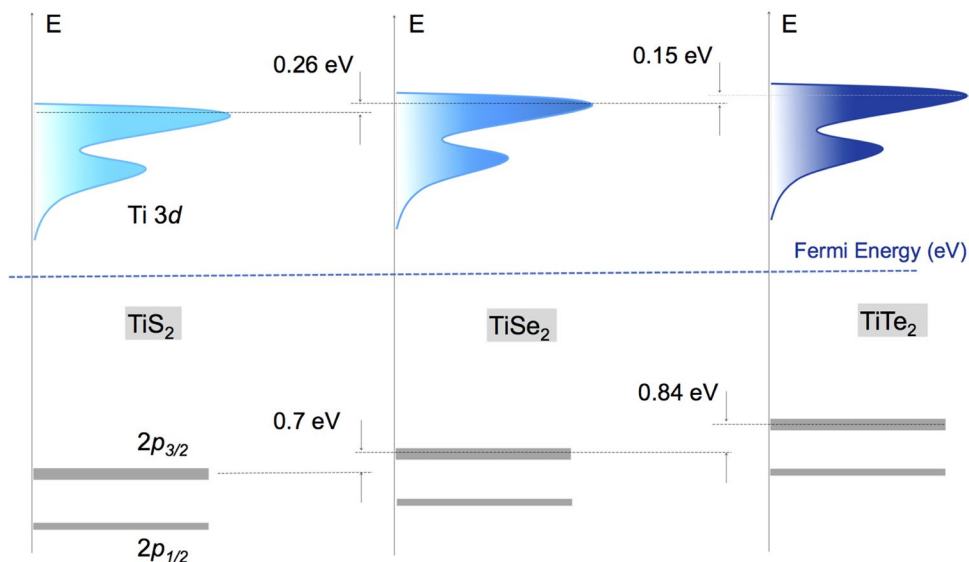
Figure 3. (**a**) Band alignment of $2p$ and $3d$ states in TiS_2, $TiSe_2$ and $TiTe_2$ as obtained from X-ray photoelectron and X-ray absorption spectroscopy.
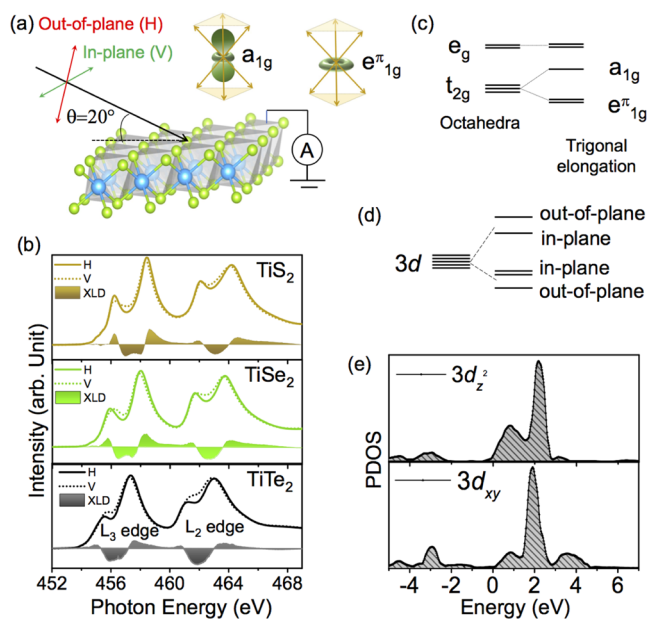
Figure 4. (**a**) Experimental setup of the in-plane and out-of-plane polarization dependent XAS measurements. (**b**) Ti $L_{3,2}$ edge XAS/XLD spectra of three different TiX_2 compounds at room temperature. (**c**) Conventional theoretical model of an elongated trigonal distortion with t_{2g} sub-band splitting. (**d**) Experimentally observed Ti $3d$ sub-band splitting in TiX_2. (**e**) PDOS of $3d_{z^2}$ and $3d_{xy}/3d_{x^2-y^2}$ obtained from previous theoretical calculations[49] on TiS_2 system where x, y, z represent global co-ordinates axis as shown schematically in Fig. 1(a).

The wave function of a_{1g} and e_g^π states is a linear combination of d_{xy}, d_{yz} and d_{xz} orbitals and can be expressed as as $|a_{1g}\rangle = \frac{1}{\sqrt{3}}(|xy\rangle + |yz\rangle + |xz\rangle)$ and $|e_{g\pm}^\pi\rangle = \pm\frac{1}{\sqrt{3}}(|xy\rangle + e^{\mp 2i\pi/3}|yz\rangle + e^{\pm 2i\pi/3}|xz\rangle)$[48]. The description of the mixed a_{1g} and e_g^π states becomes simplified when one assumes z axis along the [111] direction as shown in Fig. 1(a). The wave function of the a_{1g} state has a similar shape along [111] direction as the d_{z^2} orbital along [001]; e_g^π states are perpendicular to the [111] directions and oriented in xy plane (see the shape of the a_{1g} and e_g^π orbital Fig. 4(a)).

Based on this picture, one would naively expect that in-plane polarization will largely probe e_g^π states which are at lower energy compared to the higher energy a_{1g} state that are more sensitive to out-of-plane polarization. Contrary to this expectation, the experimental spectra for all three systems are in complete variation with the conventional picture. More specifically, in the case of t_{2g} states labeled by feature I and III in Fig. 2(c), the out-of-plane polarization (shown by solid line in Fig. 4(b)) exhibits a lower energy peak position compared to the

in-plane polarization (shown by dotted line). This implies the stabilization of a_{1g} as the lowest occupied orbital contrary to the expected e_g^{π} state. This is completely opposite to what one would infer from the standard crystals field splitting arguments. The crystal field inversion picture is schematically shown in Fig. 4(d) (Quantitative Sub-band splitting of each TiX$_2$ compound has been shown schematically in Supporting Information). These findings clearly suggest that purely ionic picture which is normally very efficient in capturing the excitation spectra of Ti^{4+} derived states in oxide systems is inadequate in explaining the origin of XLD signal in dichalcogenides. Several factors might be responsible for such discrepancy in the description of the XAS spectra. Because of the markedly enlarged p-orbitals in S, Se and especially Te, unlike oxides, covalency may play a dominant role in transition metal dichalcogenides. The synergistic effect of high metal-ligand hybridization and significant ligand field can strongly affect the local electronic description of these systems.

Adding more to the surprising finding, the crystal field splitting gap (10 Dq) between t_{2g} and e_g is found to be strongly dependent on the direction of polarization of the incident light. In particular, out-of-plane polarization (solid line in Fig. 4(b)) shows a higher crystal field gap compared to in-plane polarizations (dotted line in Fig. 4(b)). This is unexpected since for the trigonal distortion, the e_g states should not experience any sub-band splitting. However, the energy position of the e_g state is found to depend strongly on the types of polarization. All these discrepancies clearly establish that conventional crystal field picture fails to explain the observed features in these system contrary to the Ti^{4+} based oxide materials.

To resolve this inconsistency, the XAS spectra were compared with calculated projected partial density of states (PDOS) of $3d_{z^2}$ and $3d_{xy}$ states of TiS$_2$[45,49–51] as shown in Fig. 4(e). Interestingly, the calculated PDOS of $3d_{z^2}$ of titanium exhibit a double hump structure analogous to the experiments when the systems were probed with out-of-plane polarization and PDOS of the $3d_{xy}/3d_{x^2-y^2}$ states (these two states are degenerate) also shows a double hump feature similar to in-plane polarization. Moreover, the energy gap between the doublet features is greater in the case of $3d_{z^2}$ PDOS as compared to $3d_{xy}$, and $3d_{x^2-y^2}$ PDOS which is remarkably similar to the experimentally observed trend. The calculated PDOS is qualitatively consistent with experimental observations and explains the appearance of the all features and their energy position as observed from experiments. The key feature of the theoretical calculation is the inclusion of strong metal-chalcogen hybridization which is responsible for the observed crystal field inversion and allows to capture the details of electronic structure within the band-like description. This result implies that indeed covalency and metal-ligand hybridization are critical for the electronic properties of the TiX$_2$ family of materials.

In conclusion, detailed polarization dependent XAS measurements were carried out to probe and microscopically understand the effect of trigonal lattice distortion on the electronic structure of the TiX$_2$ family. All systems were characterized to rule out the presence of anion vacancies in these compounds. XLD spectra demonstrate the failure of conventional crystal field arguments in explaining the observed experimental features implying the crucial importance of covalency/metal-ligand hybridization in defining the electronic structure. Orbital projected DOS successfully reproduced the spectral features observed in our experiments. The excellent agreement between theory and the XAS spectra suggests the importance of the band-like description including trigonal lattice deformations, electron-electron correlations and metal-ligand covalency to elucidate the electronic structure of transition metal dichalcogenides.

Methods

XPS measurements. Ti 2p, S 2p, Se 3d and Te 3d core level XPS measurements were carried out in a lab-based Thermo Scientific X-ray Photoelectron Spectrometer furnished with a monochromatic Al K_α photon source and a hemi-spherical analyser with total energy resolution close to 0.45 eV. The base pressure of the main chamber was below 2×10^{-8} mbar during XPS measurements. All three TiX$_2$ compounds were mechanically exfoliated just before XPS measurements to avoid any surface contamination. The bulk sensitivity of the measurements was increased by collecting the ejected photoelectrons in a surface normal geometry. Photon energy of the source was calibrated using C 1s core level spectra with a characteristic peak at around 284.6 eV binding energy. Each core level spectrum was decomposed in a casaXPS software using Gaussian-Lorentz type line profile.

XAS /XLD measurements. XAS/XLD measurements on three TiX$_2$ compounds were carried out at Ti L$_{3,2}$ edge at beamline 4.0.2 of the Advanced Light Source (ALS), at Lawrence Berkeley National Laboratory, USA. To avoid surface contamination, each single crystal was exfoliated mechanically in nitrogen atmosphere just before carrying out XAS measurements. No further surface treatments were performed as like vacuum heating or sputtering to clean the surface as these techniques could produce chalcogen vacancy in our systems. Total electron yield (TEY) detection technique were used during the XAS/XLD measurements.

References
1. Castro Neto, A. H., Guinea, F., Peres, N. M. R., Novoselov, K. S. & Geim, A. K. The electronic properties of graphene. *Rev. Mod. Phys.* **81**, 109 (2009).
2. Allen, M. J., Tung, V. C. & Kaner, R. B. Honeycomb Carbon: A Review of Graphene. *Chem. Rev.* **110**, 132–145 (2010).
3. Kumar, S. & Chatterjee, K. Comprehensive Review on the Use of Graphene-Based Substrates for Regenerative Medicine and Biomedical Devices. *ACS Appl. Mater. Interfaces* **8**, 16431–26457 (2016).
4. Frazier, A. B., Warrington, R. O. & Friedrich, C. The Miniaturization Technologies: Past, Present, and Future. *IEEE Trans. Ind. Appl.* **42**, 423–430 (1995).
5. Gong, C. *et al.* Band alignment of two-dimensional transition metal dichalcogenides: Application in tunnel field effect transistors. *Appl. Phys. Lett.* **103**, 053513 (2013).
6. Podzorov, V., Gershenson, M. E., Kloc, C., Zeis, R. & Bucher, E. High-mobility field-effect transistors based on transition metal dichalcogenides. *Appl. Phys. Lett.* **84**, 3301–3303 (2004).
7. Xia, F., Wang, H., Xiao, D., Dubey, M. & Ramasubramaniam, A. Two-dimensional material nanophotonics. *Nat. Photonics* **8**, 899–907 (2014).

8. Mak, K. F. & Shan, J. Photonics and optoelectronics of 2D semiconductor transition metal dichalcogenides. *Nat. Photonics* **10**, 216–226 (2016).
9. Wang, Q. H., Zadeh, K. K., Kis, A., Coleman, J. N. & Strano, M. S. Electronics and optoelectronics of two-dimensional transition metal dichalcogenides. *Nat. Nanotechnol.* **7**, 699–712 (2012).
10. Baugher, B. W. H., Churchill, H. O. H., Yang, Y. & Jarillo-Herrero, P. Optoelectronic devices based on electrically tunable p-n diodes in a monolayer dichalcogenide. *Nat. Nanotechnol* **9**, 262–267 (2014).
11. Bernardi, M., Palummo, M. & Grossman, J. C. Extraordinary Sunlight Absorption and One Nanometer Thick Photovoltaics Using Two-Dimensional Monolayer Materials. *Nano Lett.* **13**, 3664–3670 (2013).
12. Britnell, L. *et al.* Strong Light-Matter Interactions in Heterostructures of Atomically Thin Films. *Science* **340**, 13111314 (2013).
13. Wi, S. *et al.* Enhancement of Photovoltaic Response in Multilayer MoS_2 Induced by Plasma Doping. *ACS Nano* **8**, 5270–5281 (2014).
14. Tsutsumi, K. X-ray-diffraction study of the periodic lattice distortion associated with a charge-density wave in $1T-VSe_2$. *Phys. Rev. B* **26**, 5756 (1982).
15. Woolley, A. M. & Wexler, G. Band structures and Fermi surfaces for $1T-TaS_2$, $1T-TaSe_2$ and $1T-VSe_2$. *J. Phys. C* **10**, 2601–2616 (1977).
16. Xi, X. *et al.* Strongly enhanced charge-density-wave order in monolayer $NbSe_2$. *Nat. Nanotechnol* **10**, 765–769 (2015).
17. Zhu, P. *et al.* Dynamic separation of electron excitation and lattice heating during the photoinduced melting of the periodic lattice distortion in $2H-TaSe_2$. *Appl. Phys. Lett.* **103**, 071914 (2013).
18. Dai, J. *et al.* Microscopic evidence for strong periodic lattice distortion in two-dimensional charge-density wave systems. *Phys. Rev. B* **89**, 165140 (2014).
19. Ingle, K. E. *et al.* Importance of structural distortions in enhancement of transition temperature in $FeSe_{1-x}Te_x$ superconductors. *Supercond. Sci. Technol* **28**, 015015 (2015).
20. Zhong, H.-X., Gao, S., Shi, J.-J. & Yang, L. Quasiparticle band gaps, excitonic effects, and anisotropic optical properties of the monolayer distorted 1 T diamond-chain structures ReS_2 and $ReSe_2$. *Phys. Rev. B* **92**, 115438 (2015).
21. Deng, K. *et al.* Experimental observation of topological Fermi arcs in type-II Weyl semimetal $MoTe_2$. *Nat. Phys* **12**, 1105–1110 (2016).
22. Bahramy, M. S. *et al.* Ubiquitous formation of bulk Dirac cones and topological surface states from a single orbital manifold in transition-metal dichalcogenides. *Nat. Mater.* **17**, 21–28 (2018).
23. Rüegg, A., Mitra, C., Demkov, A. A. & Fiete, G. A. Lattice distortion effects on topological phases in $(LaNiO_3)_2/(LaAlO_3)_N$ heterostructures grown along the [111] direction. *Phys. Rev. B* **88**, 115146 (2013).
24. Kargarian, M., Wen, J. & Fiete, G. A. Competing exotic topological insulator phases in transition-metal oxides on the pyrochlore lattice with distortion. *Phys. Rev. B* **83**, 165112 (2011).
25. Yang, B.-J. & Kim, Y. B. Topological insulators and metal-insulator transition in the pyrochlore iridates. *Phys. Rev. B* **82**, 085111 (2010).
26. Chen, P. *et al.* Charge density wave transition in single-layer titanium diselenide. *Nat Commun.* **6**, 8943 (2015)
27. Gu, Y., Katsura, Y., Yoshino, T., Takagi, H. & Taniguchi, K. Rechargeable magnesium-ion battery based on a $TiSe_2$-cathode with d-p orbital hybridized electronic structure. *Sci. Rep* **5**, 12486 (2015).
28. Sun, X., Bonnick, P. & Nazar, L. F. Layered TiS_2 Positive Electrode for Mg Batteries. *ACS Energy Lett* **1**, 297–301 (2016).
29. Lv, R. *et al.* Transition Metal Dichalcogenides and Beyond: Synthesis, Properties, and Applications of Single- and Few-Layer Nanosheets. *Acc. Chem. Res.* **48**, 56–64 (2015).
30. Whittingham, M. S. Chalcogenide battery. *US Patent No.* 4,009,052 (1977).
31. Chianelli, R. R., Scanlon, J. C. & Thompson, A. H. Structure refinement of stoichiometric TiS_2. *Mater. Res. Bull.* **10**, 1379–1382 (1975).
32. Arnaud, Y. & Chevreton, M. Etude comparative des composés TiX_2 (X = S, Se, Te). Structures de $TiTe_2$ et TiSeTe. *J. Solid State Chem.* **39**, 230–239 (1981).
33. Ishioka, J. *et al.* Chiral Charge-Density Waves. *Phys. Rev. Lett.* **105**, 176401 (2010).
34. Castellan, J.-P. *et al.* Chiral Phase Transition in Charge Ordered $1T-TiSe_2$. *Phys. Rev. Lett.* **110**, 196404 (2013).
35. Cercellier, H. *et al.* Evidence for an Excitonic Insulator Phase in $1T-TiSe_2$. *Phys. Rev. Lett.* **99**, 146403 (2007).
36. Wilson, J. A. Modelling the contrasting semimetallic characters of TiS_2 and $TiSe_2$. *Physica status solidi (b)* **86**, 11–36 (1978).
37. Wilson, J. A. Concerning the semimetallic characters of TiS_2 and $TiSe_2$. *Solid State Commun.* **22**, 551–553 (1977).
38. Hughes, H. P. Structural distortion in $TiSe_2$ and related materials-a possible Jahn-Teller effect? *J. Phys. C: Solid State Physics* **10**, L319–L323 (1977).
39. Rossnagel, K., Kipp, L. & Skibowski, M. Charge-density-wave phase transition in $1T-TiSe_2$ Excitonic insulator versus band-type Jahn-Teller mechanism. *Phys. Rev. B* **65**, 235101 (2002).
40. Bianco, R., Calandra, M. & Mauri, F. Electronic and vibrational properties of $TiSe_2$ in the charge-density-wave phase from first principles. *Phys. Rev. B* **92**, 094107 (2015).
41. Rohwer, T. *et al.* Collapse of long-range charge order tracked by time-resolved photoemission at high momenta. *Nature* **471**, 490–493 (2011).
42. Wu, Z. Y., Ouvrard, G., Moreau, P. & Natoli, C. R. Interpretation of preedge features in the Ti and S K-edge x-ray-absorption near-edge spectra in the layered disulfides TiS_2 and TaS_2. *Phys. Rev. B* **55**, 9508 (1997).
43. Wan, C. *et al.* Flexible n-type thermoelectric materials by organic intercalation of layered transition metal dichalcogenide TiS_2. *Nat. Mater.* **14**, 622–627 (2015).
44. Bullett, D. W. Electronic band structure and bonding in transition metal layered dichalcogenides by atomic orbital methods. *J. Phys. C: Solid State Phys.* **11**, 4501–4514 (1978).
45. Shkvarin, A. S. *et al.* Electronic structure of titanium dichalcogenides TiX_2 (X = S, Se, Te). *Journal of Expt. and Theo. Phys* **114**, 150–156 (2012).
46. Stavitski, E. & de Groot, F. M. F. The CTM4XAS program for EELS and XAS spectral shape analysis of transition metal L edges. *Micron* **41**, 687–694 (2010).
47. Wilson, J. A. & Yoffe, A. D. The transition metal dichalcogenides discussion and interpretation of the observed optical, electrical and structural properties. *Adv. Phys.* **18**, 193–334 (1969).
48. Khomskii, D. I. *Transition Metal Compounds* (Cambridge University Press).
49. Simunek, A., Sipr, O., Bocharov, S., Heumann, D. & Drager, G. Unoccupied electron states of TiS_2 studied by means of polarized x-ray absorption. *Phys. Rev. B* **56**, 12232 (1997).
50. Clerc, D. G. & Poshusta, R. D. Periodic Hartree-Fock Study of TiS_2. *J. Phys. Chem.* **100**, 15735 (1996).
51. Fang, C. M., de Groot, R. A. & Haas, C. Bulk and surface electronic structure of $1T-TiS_2$ and $1T-TiSe_2$. *Phys. Rev. B* **56**, 4455 (1997).

Acknowledgements

Author Contributions

B.P., Y.C. and J.C. have initiated the project. X.L., F.W. and M.K. has performed crystal characterization. B.P. has performed X.P.S. measurements. Y.C., X.L., A.T.N.D., P.S. and E.A. has carried out the XAS measurements. All authors have discussed the results of the studies. B.P., Y.C., X.L. and J.C. co-wrote the paper. All authors have commented on the manuscript.

Additional Information

Supplementary information accompanies this paper at https://doi.org/10.1038/s41598-018-37248-5.

Competing Interests: The authors declare no competing interests.

Publisher's note: Springer Nature remains neutral with regard to jurisdictional claims in published maps and institutional affiliations.